PROCEEDINGS OF SCIENCE

Nuclear pairing from microscopic forces: singlet channels and higher-partial waves

P. Finelli*
Department of Physics and Astronomy, University of Bologna (Italy) and INFN, Bologna section (Italy)
E-mail: paolo.finelli@unibo.it

In a recent paper [1] we studied the behaviour of the pairing gaps Δ_F as a function of the Fermi momentum k_F for neutron and nuclear matter in all relevant angular momentum channels where superfluidity is believed to naturally emerge. The calculations employed realistic chiral nucleon-nucleon potentials [2, 3] with the inclusion of three-body forces and self-energy effects. In this contribution, after a detailed description of the numerical method we employed in the solution of the BCS equations, we will focus our attention to the cutoff dependence of the pairing gaps and Cooper pair wavefunctions.

The Modern Physics of Compact Stars 2015
30 September 2015 - 3 October 2015
Yerevan, Armenia

*Speaker.

PoS(MPCS2015)004

1. Introduction

The goal of this article is to solve and analyze the BCS equations starting from modern nucleon-nucleon (NN) forces based on chiral effective field theory [2, 3, 4, 5].

The paper is organized as follows. Section 2 introduces the BCS theory that is the standard framework for a microscopic description of nucleonic pairing. In particular, the numerical implementation first introduced by Khodel *et al.* [6] will be reviewed in Sect. 2.4. Section 3 describes our predictions for pairing gaps in the singlet and in the coupled channel cases. Section 4 shows results of some preliminary calculations of the Cooper pair wavefunction.

2. BCS theory

2.1 Cooper pair instability

In 1956 Leon Cooper [7] was the first to understand that introducing a weak attractive interaction between pair of fermions (see case (**a**) in Fig. 1) makes the ground state of a degenerate Fermi gas at zero temperature unstable, no matter how small is the interaction[1].

What Cooper found is that such Fermi system is unstable with respect to formation of a coherent state of pairs. It is well known from elementary quantum mechanics that two particles in three dimensions can not form a bound state unless the attractive potential is strong enough. As a consequence, to understand Cooper pair formation is crucial to appreciate an important feature: the reduction from three (3D) to two spatial dimensions (2D) in the description of the problem. Because only particles near the Fermi surface are subject to pair condensation, the relevant physics is confined essentially to a 2D shell around the Fermi surface (see case (**b**) in Fig. 1 where particles belonging to the Fermi sea do not participate in the formation of the Cooper pairs and contribute to stabilize the ground state). Pairing interaction is usually weak enough that radius of pairs is larger than the interparticle distance.

The Cooper pair concept is at the basis of the Bardeen-Cooper-Schrieffer (BCS) description of superconductivity [8, 9] and in many other physical systems where *pairing*-like interactions play a dominant role.

Concerning atomic systems, Cooper pairs are usually formed by two electrons in a singlet state, i.e. where the particle spins are antiparallel with total spin $S = 0$. This is a natural consequence of the Pauli exclusion principle if electrons belong to a s orbital state ($L = 0$). Spin triplet states requires that the two fermions forming a Cooper pair must have a non-zero orbital angular momentum, i.e. $L = 1$ which is the case of superfluid states of liquid ^{3}He [10]. In nuclear physics, things are more involved by the fact that the anti-symmetrization of the Cooper pair should also consider the isospin degree of freedom. As a consequence for $L = 0$ one could observe pairing

[1] L. Cooper found that the ground-state energy of a degenerate Fermi gas with an attractive interaction between pairs of electrons on top of a quiescent Fermi sphere is, in the weak coupling regime,

$$E \simeq 2E_F - 2\omega \exp(-2/\nu(E_F)V)\,, \tag{2.1}$$

where pairs form a bound state even if the interaction V is arbitrarily small and the energy of the bound state is non-perturbative in $\nu(E_F)V$, where $\nu(E_F)$ is the density of states.

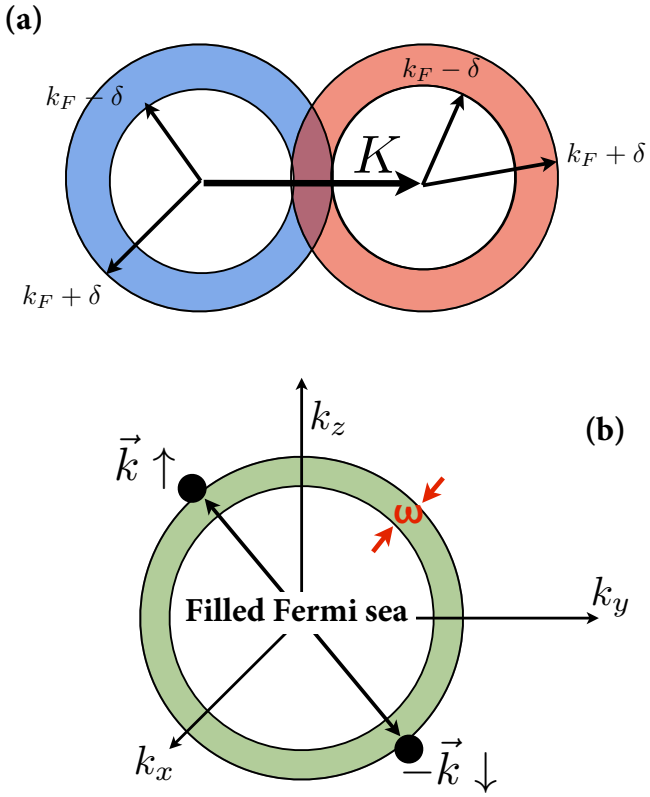

Figure 1: (**a**) Since the total momentum of the pair must be conserved, it is evident that the amount of phase space available for transition from one state to another state, of given total momentum, is a strong function of the total momentum. If the particles are confined to the region $k_F - \delta \leq k \leq k_F + \delta$, it becomes maximum when the total momentum $\boldsymbol{K} = 0$. (**b**) Cooper pairs are formed by fermions belonging to a thin energy shell ($E_F^0 - \omega < E < E_F^0 + \omega$) where particles in the Fermi sea do not participate to the dynamics.

effects both in the ${}^1S_0$ channel (with the two nucleons in an isospin triplet state $T = 1$) and in the ${}^3S_1$ channel (in an isospin singlet state $T = 0$).

2.2 BCS ansatz

BCS theory, firstly proposed to describe superconductivity in metals from a microscopic point of view, turned out to be very useful to understand superfluidity in nuclear systems [11]. In fact, in nuclear physics one can introduce a BCS-like *ansatz*

$$|BCS\rangle = \prod_{k\geq 0} \left(u_k + v_k a_k^\dagger a_{\bar{k}}^\dagger\right)|0\rangle \,, \tag{2.2}$$

where $|0\rangle$ denotes the filled Fermi sea state, while u_k and v_k represent the variational parameters (conveniently normalized with the requirement that $|u_k|^2 + |v_k|^2 = 1$). For each state $k > 0$ there always exists a conjugate state $\bar{k} < 0$. As a consequence, the $|BCS\rangle$ state is a superposition of

different number of pairs

$$|BCS\rangle \sim |0\rangle + \sum_{k>0} \frac{v_k}{u_k} a_k^\dagger a_{\bar{k}}^\dagger |0\rangle + \frac{1}{2} \sum_{kk'>0} \frac{v_k}{u_k} \frac{v_{k'}}{u_{k'}} a_k^\dagger a_{\bar{k}}^\dagger a_{k'}^\dagger a_{\bar{k}'}^\dagger |0\rangle + \dots \,. \tag{2.3}$$

Of course, Eq. (2.2) can be rewritten as follows

$$|BCS\rangle \sim \exp(P^\dagger)|0\rangle = \sum_{\nu=0}^{\infty} \frac{1}{\nu!} (P^\dagger)^\nu |0\rangle \tag{2.4}$$

with the introduction of a *pair creation* operator

$$P^\dagger = \sum_{k>0} \frac{u_k}{v_k} a_k^\dagger a_{\bar{k}}^\dagger \,. \tag{2.5}$$

The BCS ansatz leads naturally to a condensate of bound pairs (a similar relation holds for bosons in a BEC state, see footnote in Sect. 4).

2.3 BCS equations

To understand the consequences of the BCS *ansatz* it is easier to start with a Hamiltonian

$$H = \sum_{k_1 k_2} t_{k_1 k_2} a_{k_1}^\dagger a_{k_2} + \frac{1}{4} \sum_{k_1 k_2 k_3 k_4} V_{k_1 k_2 k_3 k_4} a_{k_1}^\dagger a_{k_2}^\dagger a_{k_3} a_{k_4} \,, \tag{2.6}$$

comprising a one-body kinetic and a two-body potential contributions. An additional term $-\lambda \hat{N}$ has to be added to ensure particle number conservation (at the level of expectation value). λ will be identified as the chemical potential. Working out the variation

$$\delta \langle BCS | H - \lambda \hat{N} | BCS \rangle = 0 \tag{2.7}$$

leads to the following set of equations

$$2\tilde{\varepsilon}_k u_k v_k + \Delta_k (v_k^2 - u_k^2) = 0 \,, \tag{2.8}$$

$$\Delta_k = -\sum_{k'} V_{k\bar{k}k'\bar{k}'} u_{k'} v_{k'} \,, \tag{2.9}$$

$$\tilde{\varepsilon}_k = \frac{1}{2} \left(t_{kk} + t_{\bar{k}\bar{k}} + \sum_k (V_{kk'kk'} + V_{\bar{k}k'\bar{k}k'}) v_{k'}^2 \right) - \lambda \,. \tag{2.10}$$

The solution of (2.9) is a recursive relation for the energy Δ

$$\Delta_k = -\frac{1}{2} \sum_{k'>0} V_{k\bar{k}k'\bar{k}'} \frac{\Delta_{k'}}{\sqrt{\tilde{\varepsilon}_{k'}^2 + \Delta_k^2}} \,, \tag{2.11}$$

where the BCS variational parameters can be derived from the relations

$$v_k^2 = \frac{1}{2} \left(1 - \frac{\tilde{\varepsilon}_k}{\sqrt{\tilde{\varepsilon}^2 + \Delta_k^2}} \right) \,, \tag{2.12}$$

$$u_k^2 = \frac{1}{2} \left(1 + \frac{\tilde{\varepsilon}_k}{\sqrt{\tilde{\varepsilon}^2 + \Delta_k^2}} \right) \,. \tag{2.13}$$

For a finite $\Delta_F = \Delta_{k=k_F}$ there is always a reduction in energy for the paired state and states close to the Fermi surface rearrange into a condensate of pairs. Δ_F itself is a measure of the energy gain, in fact $2\Delta_F$ can be interpreted as the energy that must be provided to reach the first excited state, i.e. the energy necessary to break a Cooper pair (see Ref. [11]). Eq. (2.11) is called the **gap equation**.

2.4 Khodel's method

In this section we explain the method suggested in Ref. [6] to solve the BCS equations by partial-wave decomposition that has been proven to be stable even for small values of the gap and to require only the initial assumption of a scale factor δ (results, of course, will be δ-independent). The BCS equation reads in terms of the NN potential $V(\mathbf{k},\mathbf{k}') = \langle \mathbf{k}|V|\mathbf{k}'\rangle$ as follows

$$\Delta(\mathbf{k}) = -\sum_{\mathbf{k}'} \langle \mathbf{k}|V|\mathbf{k}'\rangle \frac{\Delta(\mathbf{k}')}{2E(\mathbf{k}')}\,, \tag{2.14}$$

with $E(\mathbf{k})^2 = \xi(\mathbf{k})^2 + |\Delta(\mathbf{k})|^2$ and $\xi(\mathbf{k}) = \varepsilon(\mathbf{k}) - \mu$, $\varepsilon(\mathbf{k})$ denotes the single-particle energy and μ is the chemical potential. We can decompose both the interaction and the gap function into their partial-wave components,

$$\langle \mathbf{k}|V|\mathbf{k}'\rangle = 4\pi \sum_l (2l+1) P_l(\hat{\mathbf{k}}\cdot\hat{\mathbf{k}}') V_l(k,k') \tag{2.15}$$

$$\Delta(\mathbf{k}) = \sum_{lm} \sqrt{\frac{4\pi}{2l+1}} Y_{lm}(\hat{\mathbf{k}}) \Delta_{lm}(k)\,, \tag{2.16}$$

where $Y_{lm}(\hat{\mathbf{k}})$ denotes the spherical harmonics, l and m are the quantum numbers associated with the orbital angular momentum and its projection along the z axis and $P_l(\hat{\mathbf{k}}\cdot\hat{\mathbf{k}}')$ refers to the Legendre polynomials. After performing an angle-average approximation we have the following equation for any value of l

$$\Delta_l^j(k) = \sum_{l'} \frac{(-1)^\Lambda}{\pi} \int dk'\, V_{ll'}^j(k,k') \frac{\Delta_{l'}^j(k')}{E(k')} k'^2\,, \tag{2.17}$$

where $\Lambda = 1 + (l-l')/2$, j refers to the total angular momentum $\boldsymbol{J} = \boldsymbol{l} + \boldsymbol{S}$ including spin $\boldsymbol{S}$ and now $E(k)^2 = \xi(k)^2 + \sum_{jl} \Delta_l^j(k)^2$. The angle-average approximation, firstly introduced by Baldo *et al.* in Ref. [12], has been carefully analyzed by Khodel *et al.* in Ref. [13] where the authors have shown that in such case even if the pairing gap is slightly overestimated, nonetheless it is an acceptable sacrifice in accuracy if the primary interest lies in the magnitude of the pairing effect. Gaps with different l and j are coupled due to the energy denominator but we assume that different components of the interaction act mainly on non-overlapping intervals in density. We define an auxiliary potential W according to

$$W_{ll'}(k,k') = V_{ll'}(k,k') - v_{ll'} \phi_{ll'}(k) \phi_{ll'}(k')\,, \tag{2.18}$$

where $\phi_{ll'}(k) = V_{ll'}(k,k_F)/V_{ll'}(k_F,k_F)$ and $v_{ll'} = V_{ll'}(k_F,k_F)$ so that $W_{ll'}(k,k')$ vanishes on the Fermi surface. The coupled gap equations can be rewritten as

$$\Delta_l(k) - \sum_{l'} (-1)^\Lambda \int d\tau'\, W_{ll'}(k,k') \frac{\Delta_{l'}(k')}{E(k')} = \sum_{l'} D_{ll'} \phi_{ll'}(k)\,, \tag{2.19}$$

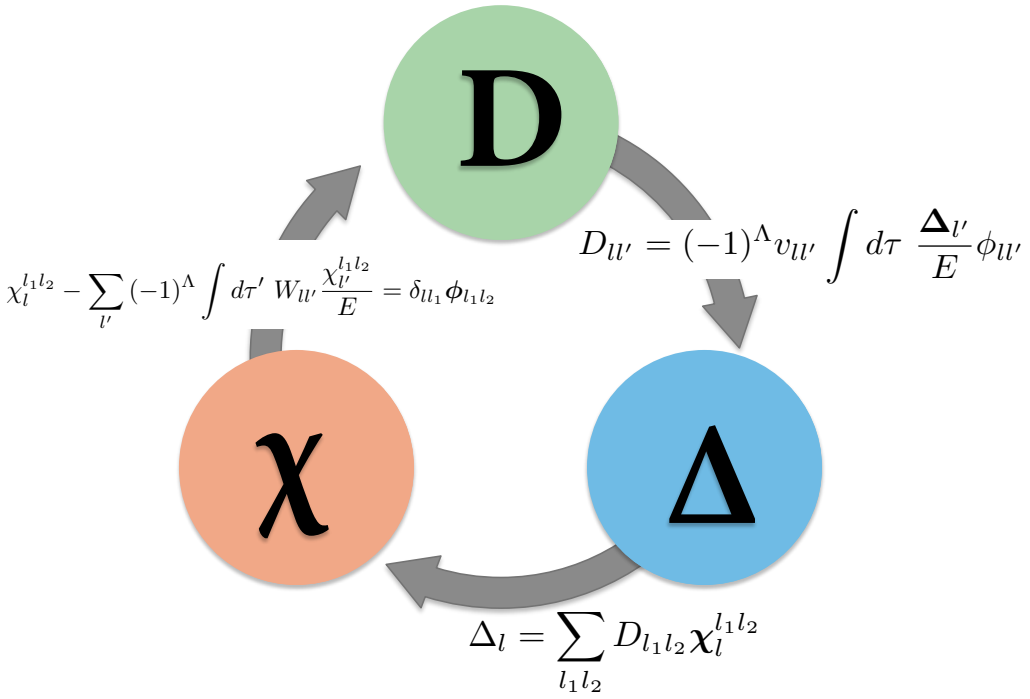

Figure 2: Self-consistent procedure (Eqs. 2.20–2.22) for the solution of the gap equation according to Khodel's prescription [6].

where $d\tau = k^2 dk/\pi$ and the coefficients $D_{ll'}$ satisfy

$$D_{ll'} = (-1)^{\Lambda} v_{ll'} \int d\tau \; \phi_{ll'}(k) \frac{\Delta_{l'}(k)}{E(k)} \,. \tag{2.20}$$

The gap is defined as follows

$$\Delta_l(k) = \sum_{l_1 l_2} D_{l_1 l_2} \chi_l^{l_1 l_2}(k) \,, \tag{2.21}$$

where

$$\chi_l^{l_1 l_2}(k) - \sum_{l'} (-1)^{\Lambda} \int d\tau' \; W_{ll'}(k,k') \frac{\chi_{l'}^{l_1 l_2}(k')}{E(k')} = \delta_{ll_1} \phi_{l_1 l_2}(k) \,. \tag{2.22}$$

The property that $W_{ll'}(k,k')$ vanishes on the Fermi surface ensures a very weak dependence of $\chi_l^{l_1 l_2}(k)$ on the exact value of the gap so that, in first approximation, it is possible to rewrite the previous equation (2.22) as

$$\chi_l^{l_1 l_2}(k) - \sum_{l'} (-1)^{\Lambda} \int d\tau' \; W_{ll'}(k,k') \frac{\chi_{l'}^{l_1 l_2}(k')}{\sqrt{\xi^2(k') + \delta^2}} = \delta_{ll_1} \phi_{l_1 l_2}(k) \,. \tag{2.23}$$

We use this equation to evaluate $\chi_l^{l_1 l_2}(k)$ initially by matrix inversion, then we use this function to self-consistently evaluate $D_{ll'}$. Finally, we solve the system given by Eqs. (2.20)–(2.22) in a self-consistent procedure as shown in Fig. 2. We always assume $\mu = \varepsilon_F$ (determining μ within the self-consistency procedure can slightly modify this relation [14]) and adopt the relativistic version of the single-particle energy $\varepsilon(k) = \sqrt{k^2 + M_N^2}$, where M_N is the nucleon mass.

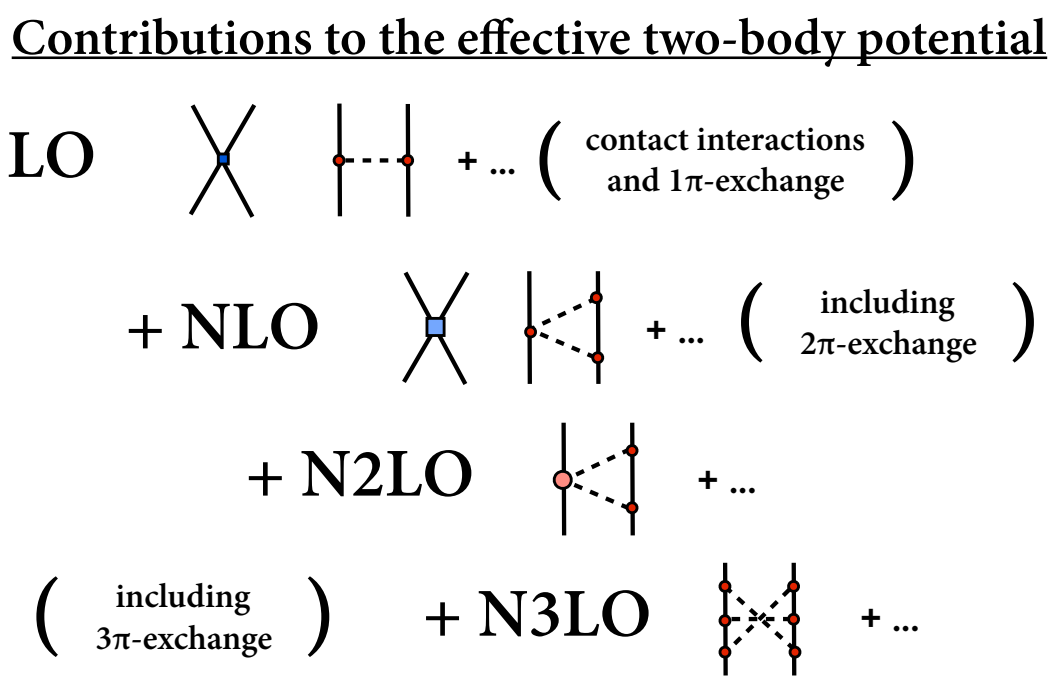

Figure 3: Schematic description of the contributions to the two-body nuclear potential in ChPT. Solid lines represent nucleons and dashed lines pions. Between parentheses short comments have been included to explain what contributions must be included order by order.

2.5 The two-body potential

In Chiral Perturbation Theory (ChPT) one identifies the appropriate low-energy degrees of freedom and derives the most general Lagrangian compatible with the symmetries and symmetry-breaking pattern of the underlying fundamental theory (i.e., QCD). The first steps towards a realistic NN potential from first principles started almost twenty years ago [15]. In this approach, the nuclear potential emerges naturally as a hierarchy of terms controlled by a power expansion in Q/Λ_χ, where Q is a soft scale (pion mass, nucleon momentum) and Λ_χ is a hard scale (nucleon mass M_N or chiral symmetry breaking scale $4\pi f_\pi$). Two-nucleon forces appear at leading order $(Q/\Lambda_\chi)^0$, while three-nucleon forces appear first at order $(Q/\Lambda_\chi)^3$, or next-to-next-to-leading order (N2LO). We employ the high-precision NN potentials developed in Ref. [2, 4, 5] at next-to-next-to-next-to-leading order (N3LO) in the chiral expansion with three choices of the Lippman-Schwinger (LS) cutoff scales ($\Lambda = 450, 500$ and 600 MeV). In Fig. 3 we show, in a very simplified way (see Fig.1 in Ref. [2] for more details), the relevant contributions to the nuclear potential in the Weinberg's power counting. At the lowest order (LO, $\sim Q^0$) the NN amplitude is made up of two contact terms and static 1π-exchange. At the next, non-vanishing, order (NLO, $\sim Q^2$) 2π-exchange terms appear for the first time in addition to new contact terms with additional spin structures. The 2π-exchange terms are finalized at order N3LO ($\sim Q^4$) with derivative seagull $\pi\pi NN$ vertices (able to include physics from intermediate $\Delta(1232)$-isobar contributions). At this order there are no new contact terms. In addition, at order N3LO ($\sim Q^4$) three-pion exchange terms are included, even if with a rather negligible contribution. Iterating the potential in a LS equation requires cutting off

high momenta components to avoid infinities. Therefore a regulator function $f(p',p)$ has to be introduced via

$$V(\boldsymbol{p},\boldsymbol{p}') \to V(\boldsymbol{p},\boldsymbol{p}')f(p',p) \tag{2.24}$$

with

$$f(p',p) = \exp\left(-(p'/\Lambda)^{2n} - (p/\Lambda)^{2n}\right) \quad \text{with} \quad n = 2 \text{ or } 3\,. \tag{2.25}$$

A method to improve NN potential's performances is a renormalization group approach [16], in particular the Similarity Renormalization Group (SRG). The main feature of the SRG is its suppression of off-diagonal momentum-space matrix elements. In this framework, one can define a class of Hamiltonians ($H = T_{rel} + V$)

$$H_s = U_s H U_s^\dagger \equiv T_{rel} + V_s\,, \tag{2.26}$$

introducing a generator

$$\eta_s = \frac{dU_s}{ds}U_s^\dagger = -\eta_s^\dagger\,, \tag{2.27}$$

with T_{rel} as the kinetic energy in terms of the relative momentum. If we may choose $\eta_s = [G_s, H_s]$, the flow equation takes the form

$$\frac{dH_s}{ds} = [[G_s,H_s],H_s]\,. \tag{2.28}$$

The SRG interaction has many salient features of low-momentum interactions, such as independence of the physical observables from the operator G_s, perturbativeness and universality. A very interesting feature of the SRG procedure is that the tensor interaction strength is reduced as s increases while leaving unchanged the corresponding phase shifts. This modification to the interaction can strongly modify the ${}^3SD_1$ gap, for instance. Since all physical observables should remain unchanged under an SRG transformation, this variation could be interpreted as an uncertainty estimate in the pairing force. A common choice for G_s is T_{rel}, and in this case as s increases, V_s approaches a diagonal form. From Eq. (2.28) it is easy to see that, if H is a two-body Hamiltonian expressed in the second quantization formalism, $(dH_s/ds)_{s=0}$ will also include three-body interactions. In this way, the evolution over the flow will naturally induce many-body interactions that must be consistently added to the *genuine* three-body forces.

3. Results

In the first panel of Fig. 4 we show the singlet channel case for neutron matter. The gap Δ_F reaches a maximum value of approximately 3 MeV at $k_F \simeq 0.85\,\mathrm{fm}^{-1}$ when the N3LO potentials are employed. In particular, the potential with a cutoff of 450 MeV produces the largest values for the gap, while the other two choices are almost equivalent. Our predictions are in rather good agreement with the gap computed from well known realistic potentials like the CD-Bonn or Nijmegen interactions [17], but at larger densities the N3LO gap exhibits a higher value. This can be explained by observing that the phase shifts from the chiral N3LO potentials exhibit more attraction than the conventional NN potential for high momenta. As shown in Ref. [1] the inclusion of three-body forces and self-energy effects reduce the size of the gap (~ 0.5 MeV) and slightly shifts the peak towards smaller densities. In the last years, this trend has been confirmed by *ab-initio* approaches [18, 19, 20].

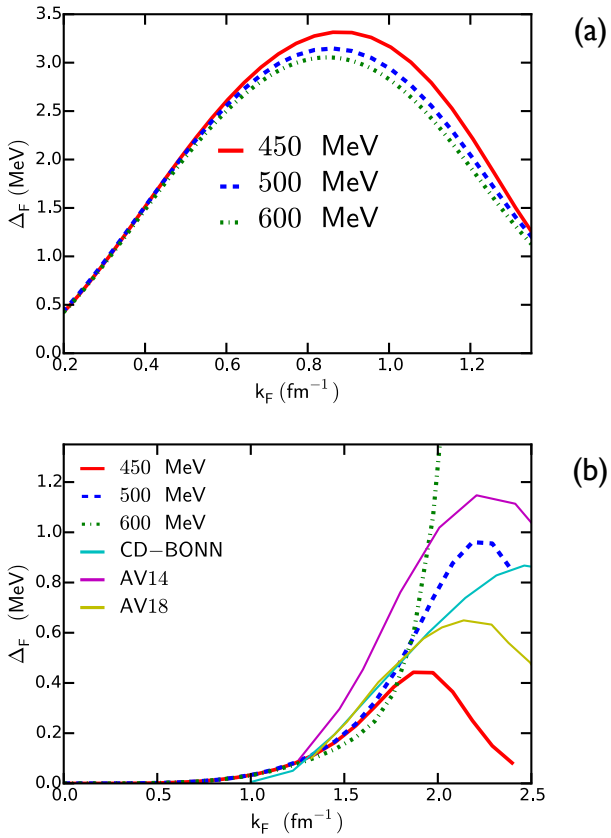

Figure 4: (**a**) The $^1S_0$ gap for neutron matter computed with the realistic chiral potentials of Ref. [2, 4, 5] at N3LO with three different LS cutoffs: 450 MeV (red line), 500 MeV (dashed blue line) and 600 MeV (green dash-dotted line). (**b**) The gap in the $^3PF_2$ channel obtained from the N3LO [2, 4, 5] interactions in comparison with several realistic NN potentials taken from Ref. [17].

In the neutron matter case, while at low density the dominant channel is the $^1S_0$ partial wave, at higher densities the high-momentum components (which are repulsive) become more important, suppressing the gap, and this happens at $k_F \approx 1.5$ fm^{-1}. At these densities, the only channel which substantially contributes to the neutron matter gap is the coupled $^3PF_2$, where the coupling is due to the tensor interaction [13, 21]. As can be seen in Fig. 4 (**b**), there is a significant dependence of the gap on the potential models (see also Ref. [17]), though the peak in the gap consistently occurs between $2.2 \leq k_F \leq 2.6$ fm^{-1}. The chiral potentials display a pronounced cutoff-dependence: if, on one hand, the 450 MeV and 500 MeV (red and blue dashed lines) give reasonable predictions in an accepted range of values, on the other hand the 600 MeV case (green dash-dotted line) does not converge and the gap curve diverges for densities above 2.0 fm^{-1}. At the high densities and associated momentum scales relevant for pairing in this channel, realistic NN interactions are not as well constained by fits to phase shifts, which partially explains the differences in the observed gaps. As explained in Ref. [2], in this channel one expects a crucial contribution from the three-pion-exchange topology at N4LO and from the contact term at N5LO, which should reduce the attraction

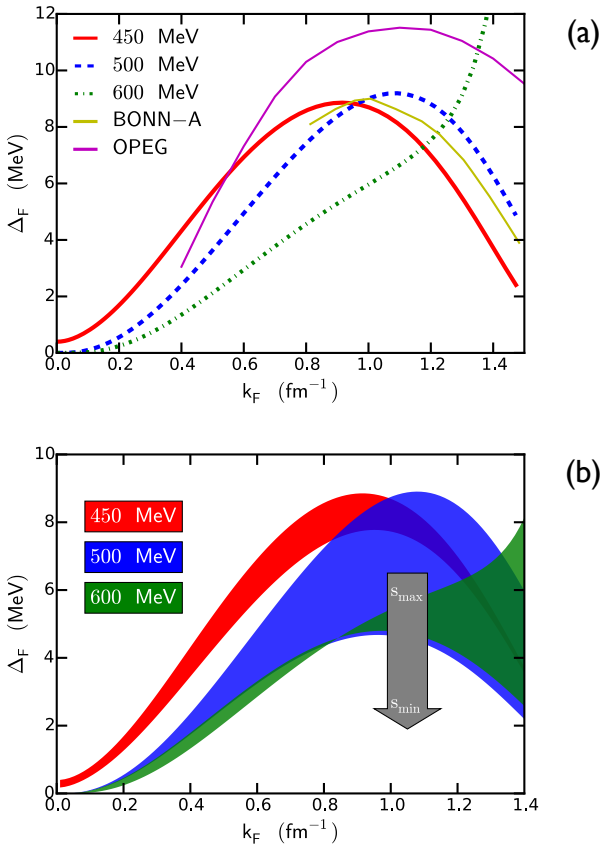

Figure 5: (**a**) The gap in the ${}^3SD_1$ channel. We plot our calculations with the N3LO interactions (red, blue dashed and green dash-dotted lines, respectively for 450, 500 and 600 MeV cutoffs) in comparison with results obtained employing BONN-A potential [23] (yellow curve) and OPEG [24] (violet line). All results suggest a very large pairing gap (around 10 MeV). (**b**) The evolution of the pairing gap in the ${}^3SD_1$ channel with SRG-evolved interactions. We employed T_{rel} as evolution operator for G_s. The arrow denote the flow variable s from larger to smaller values.

in this channel. All realistic interactions give a gap of magnitude ≤ 1 MeV, and we expect a small but not negligible reduction of the gap from the higher orders in Q/Λ_χ. The inclusion of three-body forces and self-energy effects suggests a strong reduction of the gap, as confirmed by recent *ab-initio* calculations [22].

In the nuclear matter case a non-vanishing gap appears in the ${}^3SD_1$ channel. The presence of a bound state in this channel and the very high phase shifts in the ${}^3S_1$ channel indicate that the interaction is more attractive than in the other channels. As a consequence the gap has a magnitude of about 10 MeV, as can be seen in Fig. 5 (**a**), with conventional realistic potentials.

There is no agreement on the details of the gap in this channel, but both Elgarøy *et al.* [23] and Takatsuka *et al.* [24] confirm the possibility of a gap of such magnitude (see curves labeled, respectively, by BONN-A and OPEG in the upper panel of Fig. 5). While BONN-A is a complete one-boson exchange potential, OPEG contains only the one-pion exchange tail and a Gaussian

repulsive core. As already experienced in the $^3PF_2$ case, the 450 and 500 MeV cutoffs give reasonable gaps ($\Delta_F \sim 8$ MeV) in agreement with BONN-A phenomenology, while the gap produced by the 600 MeV cutoff blows up and seems not to be under control.

The application of the SRG procedure is shown in Fig. 5 (**b**), where we tested the evolution operator $G_s = T_{rel}$. The most remarkable feature is that this procedure stabilizes the gaps produced with the higher cutoffs which basically evolve towards the same output (the maximum is reduced to approximately 5 MeV, a factor of 2 smaller compared to the bare potential). The SRG procedure is less efficient for the 450 MeV case. This behaviour could have several explanations, notably involving the tensor interaction, and deserves a dedicated analysis in a future paper.

We believe that this property must be further exploited in the future with the goal to generate a universal NN potential: a crucial ingredient for obtaining realistic pairing gaps in higher-partial waves.

4. Study of the Cooper pair wavefunctions

The Cooper pair wavefunction is defined as follows

$$\Psi_{pair} \equiv C^{'} \langle \Phi_0 | \psi^{\dagger}(\boldsymbol{r},\uparrow)\psi^{\dagger}(\boldsymbol{r}^{'},\downarrow)|\Phi_0\rangle = \frac{C}{(2\pi)^3}\int \mathrm{d}\boldsymbol{k}\, \frac{\Delta(k)}{2E(k)} e^{i\boldsymbol{k}\cdot(\boldsymbol{r}-\boldsymbol{r}^{'})}\,, \tag{4.1}$$

where $|\Phi_0\rangle$ is the BCS ground state, $\psi^{\dagger}$ is the particle creation operator and $C, C^{'}$ are normalization factors that can be fixed by imposing normalization conditions. Defining $r = |\mathbf{r} - \mathbf{r}'|$, we identify $\rho(r) = |\Psi(r)|^2 r^2$ in the singlet channel as the probability density of finding the Cooper-pair particles at a distance r from one another, assuming unit-normalization of $\Psi \equiv \Psi_{pair}$. Then $P(r) = \int_0^r ds |\Psi(s)|^2 s^2$ gives the probability density of finding these particles within a distance r of each other. Observing that the pairing gap in the S channel is larger then the one in the D channel we assumed, in the SD channel, $|\Psi(r)|^2 \approx |\Psi_{l=0}(r)|^2$ and we have approximated $\Delta(k)$ with $\Delta_{l=0}(k)$. It is now well established [14, 25, 26, 27, 28, 29, 30, 31, 32, 33] that, at low density, nuclear matter can undergo to a phase transition, belonging to the BCS-BEC crossover phenomenon [34, 35], associated with the eventual collapse of the Cooper pairs into deuteron-like particles (see Fig. 6). More than twenty years ago, Baldo *et al.* [14] observed a large overlap between the Cooper pair wavefunction and the deuteron wave function indicating that at low densities the BCS solution is hardly distinguishable from a gas of deuterons. Their conclusion was that BCS theory describes, in this peculiar density regime, a smooth transition from the SD superfluid phase of symmetric nuclear matter to the Bose Einstein condensate phase of an ideal deuteron gas.

Since BCS equations are still valid in the BEC regime [36], it is interesting to study the evolution of pairs of correlated nucleons as a function of density and spatial coordinate, starting from the solution of Eqs. (2.20–2.22). In fact the BCS wave function in the coordinate space shares some similarities to that of a Bose-Einstein condensate of a tightly bound pair of particles[2]. One of the main differences is that the ratio of the pair radius to the interparticle distance is very small in the BEC regime and very large in the BCS regime.

[2]In the BEC limit ($1/k_F a_s \gg 1$) we can approximate the pairs as point-like bosons b and the ground-state wavefunction can be written as a coherent state of these bosons: $|\Phi\rangle = C\exp(\lambda \hat{b}_0^{\dagger})|0\rangle$ where C is the normalization constant and $\lambda = \langle\Phi|\hat{b}_0^{\dagger}|\Phi\rangle$ is the order parameter.

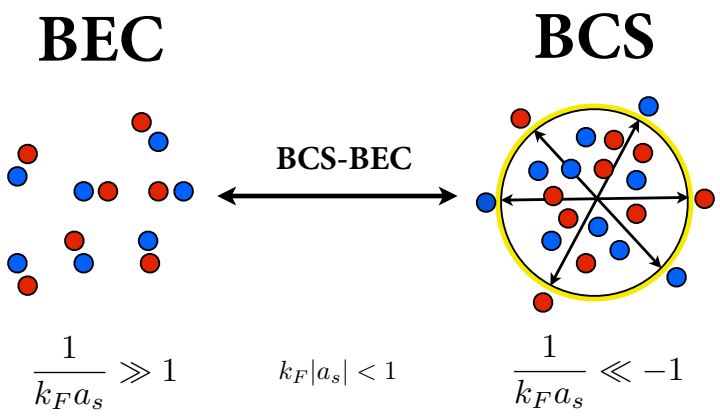

Figure 6: Crossover from BCS to BEC regimes in a two-component Fermi gas. The BCS end BEC regimes correspond respectively to the limiting cases $1/k_F a_s \gg 1$ and $1/k_F a_s \ll -1$, while the crossover region can be approximately identified by $k_F|a_s| < 1$. k_F is the Fermi momentum and a_s is the scattering length.

A few years ago, Matsuo [37] extended the previous approach to the spatial structure of a Cooper pair composed by two neutrons in superfluid low-density uniform matter. In this work, the author used two parametrizations of the BCS-BEC crossover, which serve to track the evolution of the system from the BCS to the BEC regime. These two parameters are the ratios Δ_F/ε_F and, as stated before, ξ_{RMS}/d where Δ_F and ε_F are respectively the gap and the single particle energy evaluated at the Fermi surface, $d = \rho_n^{-1/3}$ is the average distance between members of the Cooper pair and $\xi_{RMS} = \sqrt{\langle r^2 \rangle}$ is its root mean square radius of the Cooper pair. From a qualitative point of view, in the BEC regime the Cooper pair will be strongly bound ($\Delta_F \gg \varepsilon_F$) and the distance between the nucleons forming the pair will be small as compared with the average neutron distance ($\xi_{RMS} \ll d$ and $P(d) \approx 1$). The suggested values [37], as derived with a contact interaction Hamiltonian in the $^1S_0$ channel, are listed in Tab. 1.

	BCS	BEC
Δ_F/ε_F	0.21	1.33
ξ_{RMS}/d	1.1	0.19

Table 1: Reference values for $1/k_F a$ and ξ_{RMS}/d characterizing the smooth crossover between the BCS and the BEC phase, as suggested in Ref. [37] using a regularized δ interaction model.

As shown by Matsuo [37] the spatial behaviour of the neutron Cooper pair varies strongly with the Fermi momentum k_F, in particular the $\rho(r)$ profile shows strong variations. The weak-coupling limit is known to lead to an exponential falloff convoluted with an oscillation, suggesting a large correlation length. On the other hand, a pronounced peak with small oscillations could be interpreted as a signature of a transition to a different regime, i.e. of the BCS-BEC crossover. Using phenomenological pairing interactions, Matsuo [37] suggested that over a wide range of densities ($\rho/\rho_0 \simeq 10^{-4} - 0.5$) in the singlet channel the spatial dineutron correlation is strong and a possible crossover region could be found in the density range $\rho/\rho_0 \simeq 10^{-4} - 10^{-1}$.

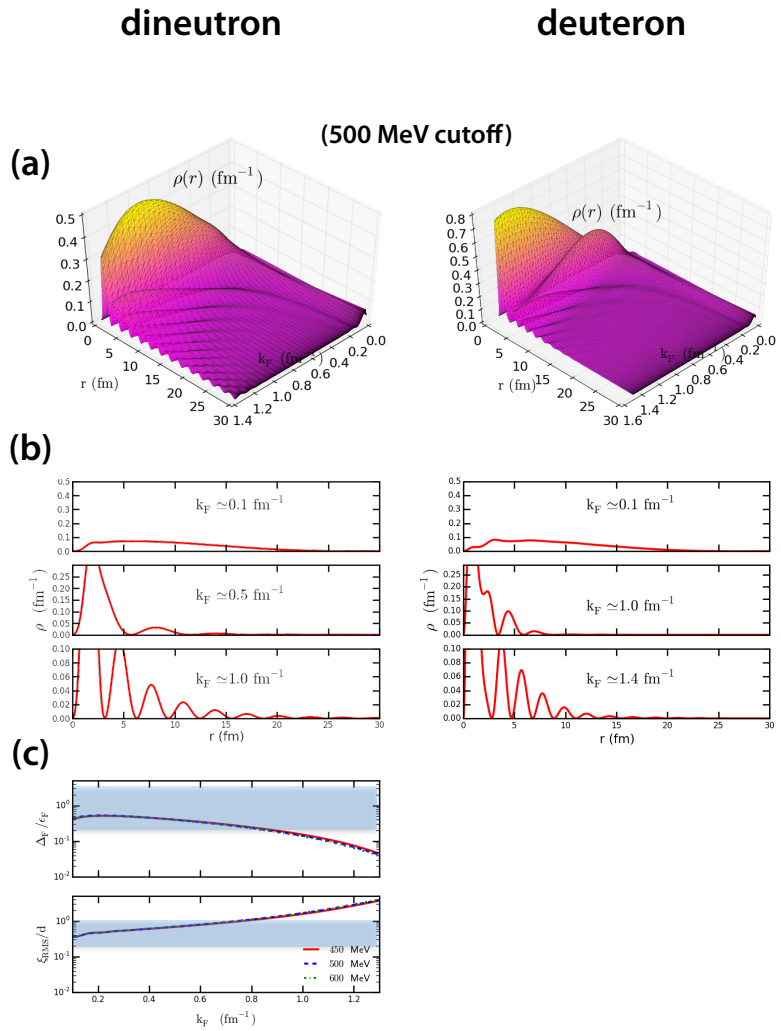

Figure 7: (**a**) Probability density ρ as function of the coordinate r and Fermi momentum k_F. **(b)** Snapshots of $\rho(r)$ for some selected values of k_F. (**c**) For dineutrons in the $^1S_0$ channel, we plot the ratios Δ_F/ε_F (upper panel) and ξ_{RMS}/d (lower panel) as functions of the Fermi momentum. The reference values characterizing the BCS-BEC crossover (see Tab. 1) define the coloured areas. In last panel, all calculations have been performed with three cutoffs: 450, 500 and 600 MeV. The cutoff dependence is practically negligible.

In Fig. 7 (**a**) we show the probability density ρ as a function of the distance variable r and Fermi momentum k_F for dineutrons in neutron matter and for deuterons in symmetric nuclear matter. For the sake of clarity we also show $\rho(r)$ for a few selected values of k_F in the graphs labelled by **(b)**. Results of Refs. [37] are substantially confirmed: we found that the profile of the dineutron probability density changes significantly with the density. At relatively small densities ($k_F < 0.8$ fm^{-1}) the system is situated in a crossover region, while at higher densities it enters the pure BCS region. The same conclusions can be obtained by observing that, at small densities, the size of the neutron Cooper pairs is small if compared with the average nucleon density, as can be seen in Fig. 7 (**c**): while for $k_F < 0.8$ fm^{-1} the pair is very compact, at higher densities the

probability to find the nucleons at great distances increases.

For deuterons, our results seem to support the previous indication [14] that the Cooper pair wave function merges smoothly into a "deuteron-like" wavefunction as density decreases ($k_F < 1.0$ fm^{-1} in our case).

Of course, the preceding results represent only a very preliminary analysis that needs to be refined and improved, i.e. including three-body forces and self-energy effects.

5. Acknowledgements

The author is deeply grateful to R. Machleidt (Physics Department, University of Idaho, Moscow) for providing the chiral potentials of Refs. [2, 4, 5]

References

[1] S. Maurizio, J. W. Holt and P. Finelli, *Nuclear pairing from microscopic forces: singlet channels and higher-partial waves*, Phys. Rev. C **90** (2014) 044003.

[2] R. Machleidt and D. R. Entem, *Chiral effective field theory and nuclear forces*, Phys. Rept. **503** (2011) 1 and references therein.

[3] E. Epelbaum, H.-W. Hammer and Ulf-G. Meissner, *Modern theory of nuclear forces*, Rev. Mod. Phys. **81** (2009) 1773 and references therein.

[4] E. Marji, A. Canul, Q. MacPherson, R. Winzer, Ch. Zeoli, D. R. Entem and R. Machleidt, *Nonperturbative renormalization of the chiral nucleon-nucleon interaction up to next-to-next-to-leading order*, Phys. Rev. C **88** (2013) 054002.

[5] F. Sammarruca, L. Coraggio, J. W. Holt, N. Itaco, R. Machleidt and L. E. Marcucci, *Toward order-by-order calculations of the nuclear and neutron matter equations of state in chiral effective field theory*, Phys. Rev. C **91** (2015) 054311.

[6] V. V. Khodel, V. A. Khodel and J. W. Clark, *Solution of the gap equation in neutron matter*, Nucl. Phys. A **598** (1996) 390.

[7] L. Cooper, *Bound electron pairs in a degenerate Fermi gas*, Phys. Rev. **104** (1956) 1189.

[8] J. Bardeen, L.N. Cooper, and J. R. Schrieffer, *Microscopic Theory of Superconductivity*, Phys. Rev. **106** (1957) 162.

[9] J. Bardeen, L. N. Cooper, and J. R. Schrieffer, *Theory of Superconductivity*, Phys. Rev. **108** (1957) 1175.

[10] A. J. Leggett, *A theoretical description of the new phases of liquid ^{3}He*, Rev. Mod. Phys. **47** (1975) 331.

[11] D. M. Brink and R. A. Broglia, *Nuclear superfluidity. Pairing in finite systems*, Cambridge Monographs on Particle Physics, United Kingdom (2010).

[12] M. Baldo, J. Cugnon, A. Lejeune and U. Lombardo, *Proton and neutron superfluidity in neutron star matter*, Nucl. Phys. A **536** (1992) 349.

[13] V. V. Khodel, V. A. Khodel and J. W. Clark, *Triplet pairing in neutron matter*, Nuc. Phys. A **679** (2001) 827.

[14] M. Baldo, U. Lombardo and P. Schuck, *Deuteron formation in expanding nuclear matter from a strong coupling BCS approach*, Phys. Rev. C **52** (1995) 975.

[15] V. Bernard, N. Kaiser and Ulf-G. Meissner, *Chiral dynamics in nucleons and nuclei*, Int. J. Mod. Phys. E **4** (1995) 193.

[16] S. K. Bogner, R. J. Furnstahl and A. Schwenk, *From low-momentum interactions to nuclear structure*, Prog. Part. Nucl. Phys. **65** (2010) 94 and references therein.

[17] M. Hjorth-Jensen and D. J. Dean, *Pairing in nuclear systems: from neutron stars to finite nuclei*, Rev. Mod. Phys. **75** (2003) 607.

[18] S. Gandolfi, A. Y. .Illarionov, F. Pederiva, K. E. Schmidt and S. Fantoni, *Equation of state of low-density neutron matter and the* $^1S_0$ *pairing gap*, Phys. Rev. C **80** (2009) 045802.

[19] A. Gezerlis and J. Carlson, *Strongly paired fermions: cold atoms and neutron matter*, Phys. Rev. C **77** (2008) 032801(R).

[20] A. Fabrocini, S. Fantoni, A. Y. Illarionov and K. E. Schmidt, $^1S_0$ *superfluid phase transition in neutron matter with realistic nuclear potentials and modern many-body theories*, Phys. Rev. Lett. **95** (2005) 192501.

[21] M. V. Zverev, J. W. Clark and V. A. Khodel, $^3P_2$-$^3F_2$ *pairing in dense neutron matter. The spectrum of solutions*, Nucl. Phys. A **720** (2003) 20.

[22] J. M. Dong, U. Lombardo and W. Zuo, $^3PF_2$ *pairing in high-density neutron matter*, Phys. Rev. C **87** (2013) 062801.

[23] Ø. Elgarøy, L. Engvik, M. Hjorth-Jensen and E. Osnes, *Minimal relativity and* $^3S_1$-$^3D_1$ *pairing in symmetric nuclear matter*, Phys. Rev. C **57** (1998) R1069.

[24] T. Takatsuka and R. Tamagaki, *Superfluidity in neutron star matter and symmetric nuclear matter*, Progr. Theor. Phys. Suppl. **112** (1993) 27.

[25] M. Serra, A. Rummel and P. Ring, *Relativistic theory of pairing in infinite nuclear matter*, Phys. Rev. C **65** (2001).

[26] U. Lombardo, P. Nozières, P. Schuck, H.-J. Schulze and A. Sedrakian, *Transition from BCS pairing to Bose-Einstein condensation in low-density asymmetric nuclear matter*, Phys. Rev. C **64** (2001) 064314.

[27] A. Sedrakian and J.W. Clark, *Pair condensation and bound states in fermionic systems*, Phys. Rev. C **73** (2006) 035803.

[28] X.-G. Huang, *BCS-BEC crossover in symmetric nuclear matter at finite temperature: pairing fluctuation and pseudogap*, Phys. Rev. C **81** (2010) 034007.

[29] T. T. Sun, B. Y. Sun and J. Meng, *BCS-BEC crossover in nuclear matter with the relativistic Hartree-Bogoliubov theory*, Phys. Rev. C **86** (2012) 014305.

[30] M. Stein, X.-G. Huang, A. Sedrakian and J. W. Clark, *Transition from BCS pairing to Bose-Einstein condensation in low-density asymmetric nuclear matter*, Phys. Rev. C **86**(2012) 062801.

[31] M. Stein, A. Sedrakian, X.-G. Huang and J. W. Clark, *Phase diagram of dilute nuclear matter: unconventional pairing and the BCS-BEC crossover*, Phys. Rev. C **90** (2014) 065804.

[32] M. Stein, A. Sedrakian, X.-G. Huang and J. W. Clark, *Spin-polarized neutron matter: critical unpairing and BCS-BEC precursor*, Phys. Rev. C **93** (2016) 015802.

[33] J. W. Clark, A. Sedrakian, M. Stein, X.-G. Huang, V. A. Khodel, V. R. Shaginyan and M. V. Zverev, *Conventional and unconventional pairing and condensates in dilute nuclear matter*, arXiv:1601.02005v1 (2016).

[34] A. J. Leggett, *Diatomic molecules and cooper pairs*, in Modern Trends in the Theory of Condensed Matter, Lecture Note in Physics **115**, Springer-Verlag Ed., Germany (1980).

[35] M. M. Parish, *The BCS-BEC crossover*, in Quantum gas experiments: exploring many-body states, World Scientific Ed., Singapore (2015).

[36] P. Pieri and G. C. Strinati, *Derivation of the Gross-Pitaevskii equation for condensed bosons from the Bogoliubov-de Gennes equations for superfluid fermions*, Phys. Rev. Lett. **91** (2003) 030401.

[37] M. Matsuo, *Spatial structure of neutron Cooper pair in low density uniform matter*, Phys. Rev. C **73** (2006) 044309.